ARMA 13-184

Coupled semi-analytical solution for CO_2 injection-induced surface uplift and caprock deflection

Chao LI
Swiss Federal Institute of Technology, EPFL, Lausanne, Switzerland
Paul BARES
Swiss Federal Institute of Technology, EPFL, Lausanne, Switzerland
Lyesse LALOUI
Swiss Federal Institute of Technology, EPFL, Lausanne, Switzerland
King Abdulaziz University, Jeddah, Saudi Arabia

This paper was prepared for presentation at the 47th US Rock Mechanics / Geomechanics Symposium held in San Francisco, CA, USA, 23-26 June 2013.

ABSTRACT: This study focuses on a specific problem related to the surface uplift induced by the injection of CO_2 at depth. The adopted methodology includes the development of a mathematical model that incorporates the deformable behaviour of storage media and the flow of two immiscible fluids (CO_2 and water) within the aquifers while the surface rock or caprock layer is modelled as a thin plate. Governing equations are solved for the axisymmetric flexural deflection due to a constant rate of injection of CO2. Comparison of the results with the surface uplift measurements (In Salah project), show good agreement. The results show that this semi-analytical solution is capable of capturing the pressure build-up during the very early stage of injection, resulting in a high rate of surface uplift. Compared to a FEM simulation, the calculation time required using the semi-analytical solution is very short; it can be employed as a preliminary design tool for risk assessment using parameters such as the injection rate, porosity, rock properties and geological structures. This semi-analytical solution provides a convenient way to estimate the influence of high injection rates of CO_2 on the surface uplift. The methodology in this development can easily incorporate other pressure distributions; thus advances in hydrology researches can also benefit this approach.

1. INTRODUCTION

Many human activities such as transportation and power generation rely on the combustion of fossil fuels. The combustion of oil, natural gas and coal accounts for about 80% of the world's energy and releases about 30 billion tonnes of carbon dioxide per year into the atmosphere [1]. Although more efficient energy alternatives are under development, the combustion of fossil fuel will continue to play an important role in the energy production for the next decades. The increased emission of carbon dioxide is believed to be responsible for global warming, which is caused by the greenhouse effect [2].

Geological sequestration of CO2 is considered as a mitigation technology to reduce carbon dioxide from entering the atmosphere by capturing and storing the CO_2 from industrial emissions. It can help limit the amount of CO_2 entering the atmosphere and the greenhouse effect, in accordance with the Kyoto Protocol, and thus allow for the continued use of fossil fuels. Deep saline aquifers are considered to be suitable geological formations for CO_2 storage because of their large capacity to trap the intended volume of CO_2 [3]. However, there are some aspects that need to be considered, such as the case of the In Salah CO_2 storage site in central Algeria; here CO_2 has been injected into a deep seated aquifer since 2004 and surface heave has been detected at a rate of up to 7mm/year around each of the three injection wells [4, 5].

Numerical investigations of this observation have been conducted by Rutqvist *et al.* [6]. The results indicate that the observed uplift at In Salah can be explained by pressure-induced poro-elastic expansion of the injection zone, which includes deformations within the sealing caprock layer just above the aquifer. In addition, the vertical displacement has a similar distribution trend as the fluid overpressure during injection, which reaches a maximum around injection well and decreases gradually with distance from the injection well [7]. Injection of

CO_2 into deep aquifers is considered as a hydromechanical coupled process [8]. High rates (>1Mt/year) of injection of CO_2 into an aquifer could result in an abrupt fluid pressure build-up within the injection area [9]. This increase in fluid pressure leads to deformation of the aquifer and the sealing caprock. Induced strain may propagate to the surface [10] and can also cause variations in the porosity resulting in alterations in the hydraulic properties such as permeability. As a consequence, the state of fluid overpressure changes further. Employing a hydromechanical coupling technique can help estimate the surface or caprock deformation more accurately.

Rutqvist [8] estimated the surface uplift at In Salah using a simple analytical solution according to [11]. The uplift is overestimated because of various assumptions such as a unique layer of the reservoir, 1-dimentional geometry and a uniformly distributed overpressure. This can be accepted as a very preliminary approximation on the order of magnitude of uplift. In reality, the contact between the rock layers is often curved, which tends to prevent the induced strain from propagating to the surface. Furthermore the uplift is highly dependant on the state of the overpressure as previously stated. It is important to incorporate the temporal and spatial evolution of the overpressure in order to determine the magnitude of the uplift.

Selvadurai [12, 13] has derived a convenient mathematical model for determining the surface uplift and caprock vertical deformation respectively. By taking in account bending effects, the axisymmetric flexural deflections of the surface layer and caprock layer have been deduced analytically. Nevertheless a flat overpressure within the injection zone is assumed in the study, which could be refined. Vilarrasa *et al.* [14] has derived expressions for fluid overpressure distributions from two analytical solutions proposed by Nordbotten *et al.* [15] and Dentz and Tartakovsky [16]. The overpressure predicted by both approaches displays a more realistic distribution and has the same order of magnitude as numerical simulations after accounting for CO_2 compressibility and viscosity [14].

The goal of this paper is to assess the surface uplift and caprock deformation by deriving a semi-analytical solution, which takes a more realistic evolution of overpressures into account. First, a mathematical analysis of the pressurization-induced displacement is given. This is followed by the incorporation of the real distribution of overpressure. After proposing several numerical simulations using the semi-analytical analysis, the solution is employed to estimate the surface uplift observed at the In Salah project as an illustrative example.

2. CAPROCK DEFORMATION DUE TO PRESSURIZATION

2.1. Embedded plate approach

Selvadurai [13] has proposed a straightforward analytical approximation to estimate the primary caprock deformation due to constant injection-induced uniformly distributed overpressures over a circular region located under the caprock layer. The proposed system consists of an overburden region and a storage unit with a primary caprock in between. CO_2 is injected into an *m*-metre-thick injection zone within a storage unit with a distance l to the primary caprock (**Figure 1**). The injection zone can be situated just below the primary caprock (l=m/2). Injection of fluids at a constant rate through a vertical injection well causes radial pressurization in the injection zone, the so-called disc-shaped pressurized zone. The approach assumes that (i) the caprock is oriented horizontally and embedded between an overburden region and a storage region, (ii) the caprock layer is considered as a thin plate and (iii) it behaves elastically. The assumption of a thin plate applied here is justified by its thickness in relation to the dimension (radius) of the pressurized zone [17]. Both overburden and storage regions are modelled as half-space regions and an isotropic elastic model is applied to these regions.

The embedded caprock layer exhibits flexural behaviour that is governed by the Germain-Poisson-Kirchhoff thin plate theory [17]. The governing equation is written in polar coordinates with the Laplace operator $\tilde{\nabla}^2 = \frac{d^2}{dr^2} + \frac{1}{r}\frac{d}{dr}$:

$$D\tilde{\nabla}^2\tilde{\nabla}^2 w(r) + q^{(s)}(r) - q^{(o)}(r) = 0 \qquad (1)$$

where the deflection $w(r)$ is constrained by contact stresses $q^{(s)}(r)$ and $q^{(o)}(r)$, which are applied on the contact faces between the caprock and respective regions. The flexural rigidity of the embedded caprock layer is expressed by $D\left(=G_c h^3/6(1-\nu_c)\right)$ with the thickness h of the caprock layer, shear modulus G_c and Poisson's ratio of the caprock ν_c. The pressurization of intensity Δp [Pa/m^3] is within a disc-shaped pressurized region with a radius of influence R and thickness m located at a distance l from the interface between the caprock and the storage region as shown in **Figure 1**. The interactions between the caprock and the adjacent regions are induced by the pressurization that can be considered as an injection pressure over the hydrostatic pressure presented in the storage region. The caprock layer is then assumed to be in bonded contact with the storage and overburden regions, of which the relevant kinematic interface conditions are:

$$w(r,z=0)=u_z^{(s)q}(r,0)+u_z^{(s)p}(r,0)=u_z^{(o)q}(r,0) \tag{2}$$

$$u_r^{(s)}(r,z=0)=u_r^{(s)p}(r,0)=u_r^{(o)}(r,0)=0 \tag{3}$$

where u_r and u_z are, respectively, the radial and axial displacement vector in the polar coordinates, u^p is the displacement due to overpressure Δp and u^q is the displacement constrained by the contact stress q.

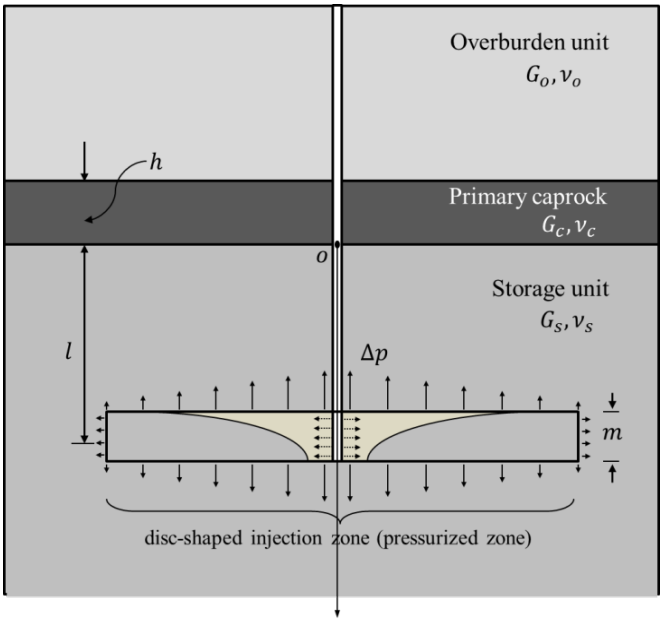

Figure 1. The idealized configuration of an embedded caprock layer.

Pressurization-induced deflection

2.2. Pressurization-induced deflection

According to Segall *et al.* [18], the surface displacement of the storage region induced by a distribution of axisymmetric overpressure can be written as:

$$u_z^{(s)p}(r,0)=\frac{\alpha_s}{G_s}\int_0^\infty\int_0^\infty \Delta p(\rho)\cdot g_z(r,z=0;\rho,d)\,\mathrm{d}\rho\,\mathrm{d}d \tag{4}$$

where

$$g_z(r,z=0;\rho,d)=-(1-2\nu_s)\rho\int_0^\infty \xi J_0(\xi r)J_0(\xi\rho)e^{-\xi d}\mathrm{d}\xi \tag{5}$$

is the Green's function, which corresponds to a ring of dilatation at radius $\rho\in[0,\infty)$ and depth $d\in\left[l-m/2,\,l+m/2\right]$.

An approximation for operating the integral is given by:

$$\int_{l-m/2}^{l+m/2} e^{-kd}\,\mathrm{d}d \approx me^{-kl} \tag{6}$$

This approximation is valid when the thickness of aquifer m is small compared to its depth l to the caprock[19]. Note that this assumption is necessary for deriving the next step of the formulation analytically; as a consequence, the assumption constrains the range of applications, for example, the case where the aquifer is situated just below the caprock ($l=m/2$). However, with the decaying behaviour of the multiplication of two Bessel functions in Eq.(5) (Appendix I), the relationship between l and m becomes less important, see Appendix II. In conclusion, the consequence of this assumption on the physical interpretation is negligible.

The integral Eq.(4) can therefore be expressed as follows:

$$u_z^{(s)p}(r,0)=-\frac{(1-2\nu_s)\alpha_s m}{G_s}\int_0^\infty \xi J_0(\xi r)e^{-\xi l}\int_0^\infty \rho\Delta p(\rho)J_0(\xi\rho)\mathrm{d}\rho\,\mathrm{d}\xi \tag{7}$$

Eq.(7) shows a linear relationship between the displacement and the material properties (i.e., $1/G_s$ and ν_s). The displacement induced by pressurization depends strongly on the Bessel integral of the overpressure function $\Delta p(\rho)$. Operating on $u_z^{(s)p}(r,0)$ with the zeroth-order Hankel transform (Appendix III) gives:

$$\overline{u}_z^{(s)p}(\xi)=-\frac{(1-2\nu_s)\alpha_s m}{G_s}\overline{\Delta p}(\xi)e^{-\xi l} \tag{8}$$

where $\overline{\Delta p}$ is the zeroth-order Hankel transform of Δp.

Selvadurai [13] stated that the displacement was constrained by the contact stresses:

$$\overline{u}_z^{(s)q}(r,0)=\frac{(3-4\nu_s)}{4G_s(1-\nu_s)}\frac{1}{\xi}\overline{q}^s(\xi) \tag{9}$$

$$\overline{u}_z^{(o)q}(r,0)=\frac{(3-4\nu_o)}{4G_o(1-\nu_o)}\frac{1}{\xi}\overline{q}^o(\xi) \tag{10}$$

Combing the kinematic constraint Eq.(2) to which the storage region is subjected, the displacement induced by the pressurization Eq.(8) and the restricted deflection caused by the contact stress Eq.(9), one can obtain the following equation after employing the zeroth-order Hankel transform:

$$\bar{q}^s(\xi)=\frac{4G_s(1-\nu_s)}{(3-4\nu_s)}\xi\bar{w}(\xi)+\frac{4(1-\nu_s)(1-2\nu)\alpha_s m}{(3-4\nu_s)}\xi\overline{\Delta p}(\xi) \tag{11}$$

Considering the kinematic constrains Eq.(2) and Eq.(10) on the storage region, we can obtain:

$$\bar{q}^o(\xi)=-\frac{4G_o(1-\nu_o)}{(3-4\nu_o)}\xi\bar{w}(\xi) \tag{12}$$

Operating on the differential equation Eq.(1) with the zeroth-order Hankel transform:

$$D\xi^4\bar{w}(\xi)+\bar{q}^s(\xi)-\bar{q}^o(\xi)=0 \tag{13}$$

and introducing Eq.(11) and Eq.(12), one can find the deflection of the caprock layer induced by an arbitrary radial pressurization after the inverse Hankel transformation:

$$w(r)=\frac{\Omega m}{h^2}\int_0^\infty\frac{\xi}{1+\Phi\xi^3}\overline{\Delta p}\left(\frac{\xi}{h}\right)e^{-\frac{\xi l}{h}}J_0\left(\frac{\xi r}{h}\right)d\xi \tag{14}$$

where Ω and Φ are constants dependant on the properties of the medium:

$$\Omega=\frac{\alpha_s(1-\nu_s)(1-2\nu_s)(3-4\nu_o)}{G_s(1-\nu_s)(3-4\nu_o)+G_o(1-\nu_o)(3-4\nu_s)} \tag{15}$$

$$\Phi=\frac{(3-4\nu_s)(3-4\nu_o)G_c}{24(1-\nu_c)\left[G_s(1-\nu_s)(3-4\nu_o)+G_o(1-\nu_o)(3-4\nu_s)\right]} \tag{16}$$

3. OVERPRESSURE INDUCED BY CO_2 INJECTION

To find the deflection w(r) according to (14), the overpressure distribution $\overline{\Delta p}$ must be incorporated. Selvadurai [12, 13] considers a constant overpressure distributed within the pressurization zone. However, CO_2 injection will result in a high concentration of overpressure around the injection well and this overpressure vanishes with the distance to the well [7]; such an overpressure pattern is necessary to estimate the magnitude of the deformation more accurately. This can be derived from two analytical solutions proposed by Nordbotten *et al.* [15] and Dentz and Tartakovsky [16], which describe the advancing interface between the injected CO_2 and host water. Both solutions consider that an abrupt interface separates the two fluids, which are assumed to be immiscible [20]. As shown in **Figure 2**, the problem formulation is divided into three regions: (1) around the injection well, only injected CO_2 exists ($r\le r_b$); (2) the intermediate region where the two fluids coexist but are separated by a sharp interface ($r_b\le r\le r_0$); (3) the outer region where only host water exists ($r_0\le r\le R$ [1]). The governing equation for the interface position can be derived as [20]:

$$\frac{1}{r}\frac{\partial}{\partial r}\left[\zeta\frac{Q_0-2\pi r(\rho_w-\rho_c)g(k/\mu_c)(m-\zeta)\partial\zeta/\partial r}{\zeta+(m-\zeta)\mu_w/\mu_c}\right]+2\pi\phi\frac{\partial\zeta}{\partial t}=0 \tag{17}$$

where Q_0 is the volumetric flux rate of injected CO_2 and ζ denotes the vertical position of the interface between two fluids. Both solutions ([15, 16]) are approximations to the exact solution of Eq.(17). Their difference comes from the assumptions they made for the approximation. While Nordbotten *et al.* [15] used an energy minimization approximation, Dentz and Tartakovsky [16] applied the Dupuit assumption of horizontal flow. The development of both solutions is not detailed in this paper; the reader is referred to the original works of Nordbotten *et al.* [15] and Dentz and Tartakovsky [16] for their approaches. In addition, the validity of both solutions has been discussed in [21, 22].

The interface equations derived by Nordbotten *et al.* [15], denoted by NB and Dentz and Tartakovsky [16], denoted by DZ, are written respectively as:

$$\zeta_{NB}(r,t)=m\left[1-\frac{\mu_c}{\mu_w-\mu_c}\left(\sqrt{\frac{\mu_w Q_0 t}{\mu_c\phi\pi m r^2}}-1\right)\right] \tag{18}$$

$$\zeta_{DZ}(r,t)=\frac{Q_0}{2\pi kmg}\frac{\mu_w-\mu_c}{\rho_w-\rho_c}\ln\left(\frac{r}{r_{b,DZ}(t)}\right) \tag{19}$$

where $r_b(t)$ is the radius at which the interface intersects the lower domain boundary and is determined by the volume conservation [16]:

$$r_{b,DZ}(t)=2\sqrt{\frac{tkmg(\rho_w-\rho_c)}{\phi(\mu_w-\mu_c)}\left[\exp\left(\frac{4\pi km^2g(\rho_w-\rho_c)}{Q_0(\mu_w-\mu_c)}\right)-1\right]^{-1}} \tag{20}$$

[1] R is the radius of influence. Injection induced overpressure is supposed to be equal to zero at R.

Plugging the interface equations (18) and (19) into the integration of Darcy's law, the overpressure expressions from the two analytical solutions are derived by Vilarrasa *et al.* [14].

Taking the overpressure equations Eq.(17) (corresponding to the solution of NB) and Eq.(19) (corresponding to the solution of DZ)) from [14], we can derive expressions for the vertically averaged overpressure for the two analytical solutions using the zeroth–order Hankel transform:

$$\overline{\Delta p}_{NT}(\xi)=\frac{A}{\xi^2}\left[y\ln\left(\frac{y}{\xi R}\right)J_1(y)+J_0(y)\right]_{\xi R}^{\xi r_0}$$
$$+A\left[\ln\left(\frac{R}{r_0}\right)+Br_0\right]\frac{r_0J_1(\xi r_0)-r_bJ_1(\xi r_b)}{\xi}$$
$$+A\left[\ln\left(\frac{R}{r_0}\right)+B(r_0-r_b)\right]\frac{r_bJ_1(\xi r_b)-r_wJ_1(\xi r_w)}{\xi}$$
$$+\frac{AC}{\xi^2}\left[y\ln\left(\frac{y}{\xi r_b}\right)J_1(y)+J_0(y)\right]_{\xi r_b}^{\xi r_w}$$
$$-AB\int_{r_b}^{r_0}r^2J_0(\xi r)dr \qquad (21)$$

with parameters $A=\frac{Q_0\mu_w}{2\pi kd}$; $B=\sqrt{\frac{\mu_c\phi\pi d}{\mu_wV(t)}}$; $C=\frac{\mu_c}{\mu_w}$ and $R=\sqrt{\frac{2.25k\rho_wgt}{\mu_wS_s}}$.

$$\overline{\Delta p}_{DT}(\xi)=\frac{A}{\xi^2}\left[y\ln(\frac{y}{R\xi})J_1(y)+J_0(y)\right]_{\xi R}^{\xi r_0}$$
$$+\frac{A}{\mu_w}\hat{B}\frac{r_0J_1(\xi r_0)-r_wJ_1(\xi r_w)}{\xi}$$
$$+\frac{A}{\mu_w}\frac{\mu_c}{\xi^2}\left[y\ln(\frac{y}{r_b\xi})J_1(y)+J_0(y)\right]_{\xi r_0}^{\xi r_w}$$
$$+\frac{A}{\mu_w}\hat{C}\int_{r_b}^{r_0}r\ln(\frac{r}{r_b})\ln(\frac{r_b}{r})J_0(\xi r)dr \qquad (22)$$

and parameters $\hat{B}=\mu_w\ln(\frac{R}{r_b})-\frac{\mu_w-\mu_c}{2\gamma}$;

$\hat{C}=\frac{(\mu_w-\mu_c)\gamma}{2}$ and $\gamma=\frac{Q_0(\mu_w-\mu_c)}{2\pi km^2g(\rho_w-\rho_c)}$.

Introducing Eqs.(21) and (22) into Eq.(14), we can obtain the CO_2 injection-induced caprock deflection, taking into consideration the real distribution of overpressure in the aquifer that has a moving interface associated with the hydrodynamic displacement of immiscible fluids. The compressibility of CO_2 is also included by the methodology proposed by Vilarrasa *et al.* [14].

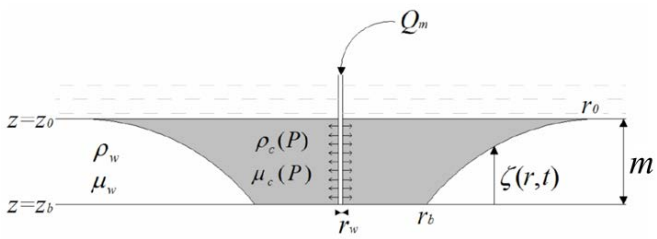

Figure 2 Injection of CO_2 into a homogeneous horizontal aquifer [14]

4. NUMERICAL APPLICATION

4.1. Case studies

The infinite integration of Eq.(14) with Eq.(21) shows an oscillatory and decaying nature, which can be achieved relatively easily with a suitable quadrature. While dealing with the integration of Eq.(14) with Eq.(22), some algebra manipulation needs to be performed to avoid oscillatory functions where the amplitude decreases too slowly towards infinity. To ensure the convergence of the integration, an appropriate number of intervals is chosen to perform the numerical calculation using Matlab®. Depending on the number of output variables, the calculation can be achieved in less than 10 seconds of CPU time per time step t and distance r.

We considered an example of a 100m thick caprock layer which is 1km underground. Through a vertical well with a radius $r_w=0.15$m, CO_2 is injected at a constant rate of 100kg/s into an *m*=100m thick aquifer, which located at a certain depth from the caprock. Material parameters are listed in **Table 1**.

The spatial distribution of overpressure is displayed in **Figure 3**. As stated in [14], the overpressure decreases with distance logarithmically in the DZ solution while it decreases linearly with the solution of NB over the region where the two fluids coexist. As expected, the overpressure calculated using the DZ solution is higher than the one using NB. The pressurization-induced deflection has the same trend as the overpressure (**Figure 4**). The curvature of the deflected shape is smoother in the case of NB around the injection well than that with the solution of DZ, which will further influence the stress development.

Figure 5 shows the relationship between the deflection of the caprock and the distance to the injection zone. As can be seen from the figure, the magnitude of the

overpressure decreases when the distance *l* is increased. The CO_2 density increases as the hydrostatic pressure increases with the depth; thus, for a given mass of injected CO2, the injected volume reduces and less overpressure is built up. Since the overpressure at the injection well is estimated to be higher using the DZ solution rather than the NB solution, a higher overpressure is obtained with DZ solution with a nearly constant difference in the magnitude. The thickness of zone between the caprock and the injection zone actually limits the strain propagating from the injection zone to the caprock. Hence the difference in the magnitude of deflection at the caprock vanishes with the distance *l* while the difference in the overpressure remains nearly constant (see **Figure 6**). The effect of the overpressure difference is most significant in the case where both layers are adjacent and it becomes negligible when *l*=400m, suggesting that injection of CO_2 at a certain distance to the primary caprock can reduce the possible strain within the caprock and further reduce the possibility of fissuring and cracking.

Temporal evolution of the caprock deflection is shown in **Figure 7** with various permeabilities. With a constant rate of injection, the fluid pressure increases dramatically at the very beginning of the injection period. As a consequence of the elastic model, the deflection reflects the effect of overpressure and shows the same behaviour. The deflection increases gradually after one year of injection and reaches a maximum. The deflection is almost proportional to the inverse of the permeability (see Eqs.(21) and (22)). Thus the permeability can be considered as an important factor to limit the overpressure build-up and subsequent deflections.

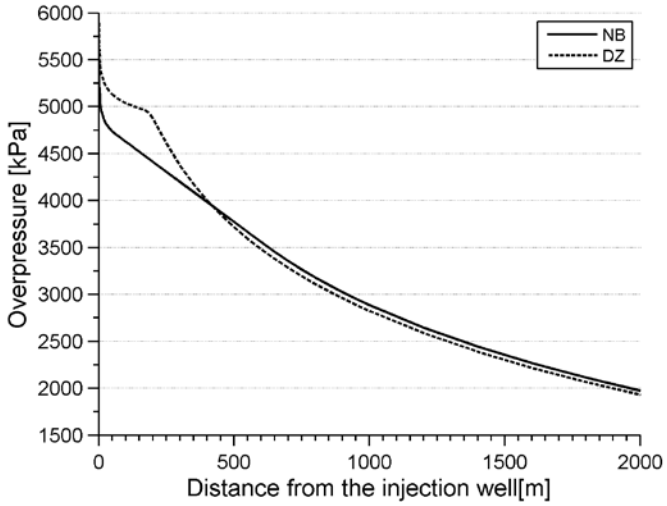

Figure 3 Spatial distribution of vertically averaged overpressure after 100 days of injection with the reference parameters

Table 1 Parameters values used in the numerical simulation

Parameter	Symbol	Unit	Overburden unit	Storage unit	Caprock layer
Shear modulus	*Go, Gs, Gc*	GPa	1	10	5
Poisson's ratio	ν_o, ν_s, ν_c	-	0.25	0.25	0.25
Porosity in the injection zone	ϕ	-		0.17	-
Permeability in the injection zone	k	m^2		1.3e-14	-
Thickness of the caprock	m	m	100		
Distance from the caprock to the middle of the injection zone	l	m	50		
Well radius	r_w	m	0.15		
Injection rate	Q_m	kg/s	100		

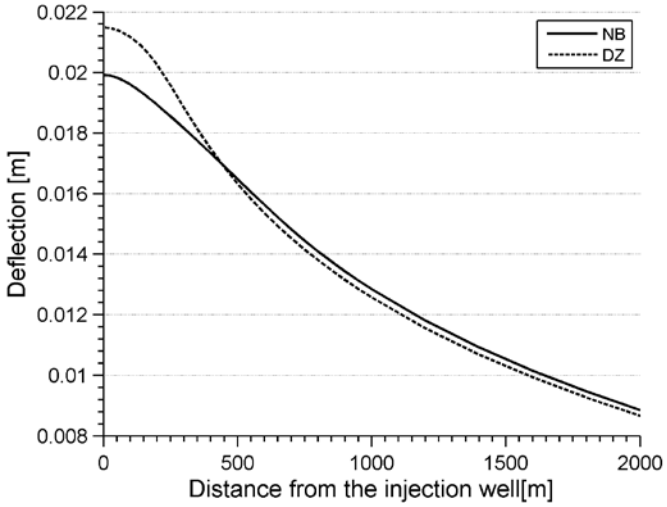

Figure 4 Spatial distribution of the deflection of the caprock after 100 days of injection with the reference parameters

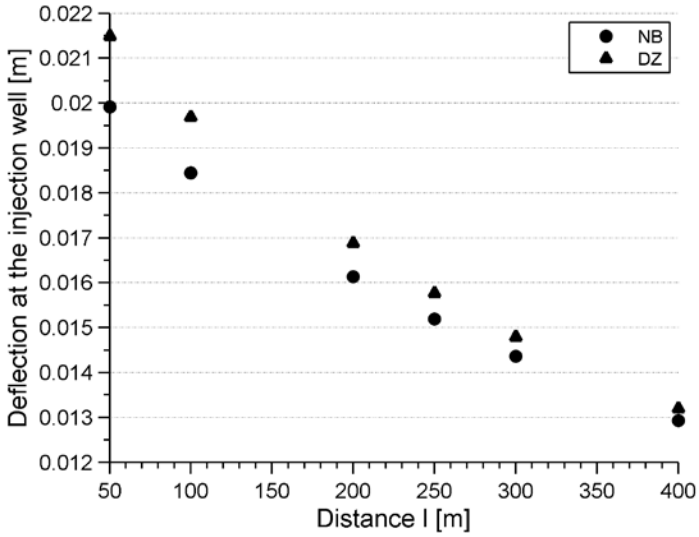

Figure 5 Maximum deflection calculated after 100 days of injection with different distances (*l*) to the interface between the caprock and the aquifer

4.2. Application to the case of the In Salah project

The injection of CO_2 into the deep aquifer at the In Salah project lead to more than 1500 micro-seismic events throughout 2009 and 2010 [23], which are believed to be generated from the cracking or fracturing of the reservoir (and possibly surrounding rocks) when the injection pressure exceeds the formation fracture pressure [24]. Surface deformation around the CO_2 injection wells at In Salah was analysed by satellite-borne SAR data [4]. Surface heave was detected around all three injection wells. Hence it is clear that this is an issue that must be handled seriously. Surface uplift at In Salah has been investigated using semi-analytical solutions [5]. Rutqvist *et al.* [6, 25] investigated the surface uplift around one specific injection well at In Salah using a 3D finite element model. The results are comparable to the field measurements. Here we apply the proposed semi-analytical approach in order to assess the surface uplift around the same injection well as in [6, 25] and compared the results to both the measured data and numerical simulations. Since the semi-analytical solution is for the purpose of a preliminary estimation, the objective here is to focus on a simple geometry case and to capture the overall behaviour of the surface deformation around the injection well.

Through the injection well KB501(**Figure 8**), the CO_2 is injected into a 20m thick water-saturated layer at a rate of about 8kg/s [6]. The injection zone is situated at 1800m underground [6]. **Figure 8**a clearly shows that a surface heave, at a rate of 5mm, has been detected. More specifically, the surface uplift reaches 10mm during the first year (**Figure 8**b).

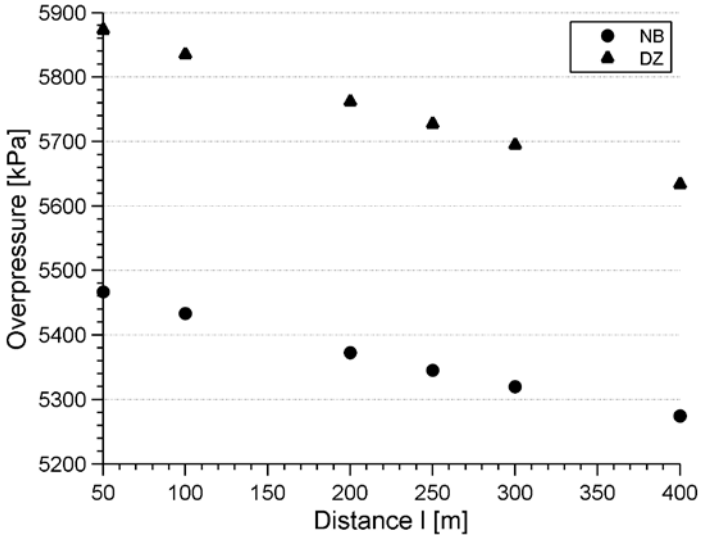

Figure 6 Vertically averaged overpressure at the injection well after 100 days of injection with different distances (*l*) to the interface between the caprock and the aquifer

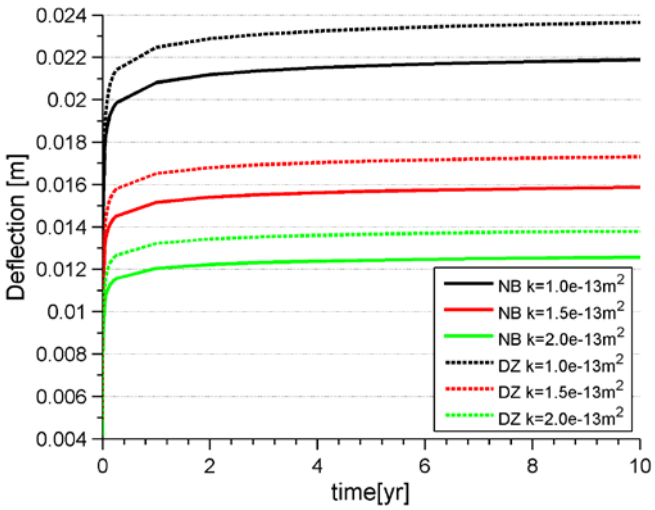

Figure 7 Deflection at the injection well with time for various permeabilities

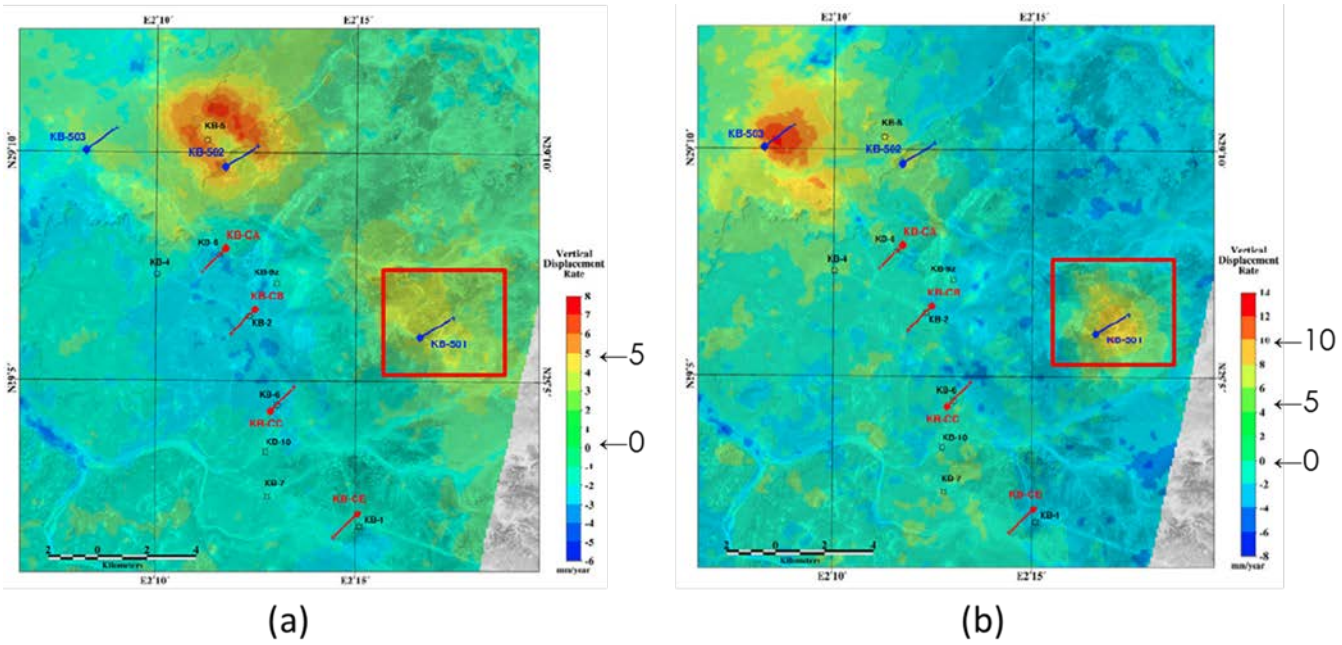

Figure 8 Vertical displacement rate of the period from (a) 2004/7/31 to 2008/5/31 and (b) 2004/7/31 to 2005/9/24 at the In Salah detected by DInSAR stacking. KB-501 is CO_2 injection well [2].

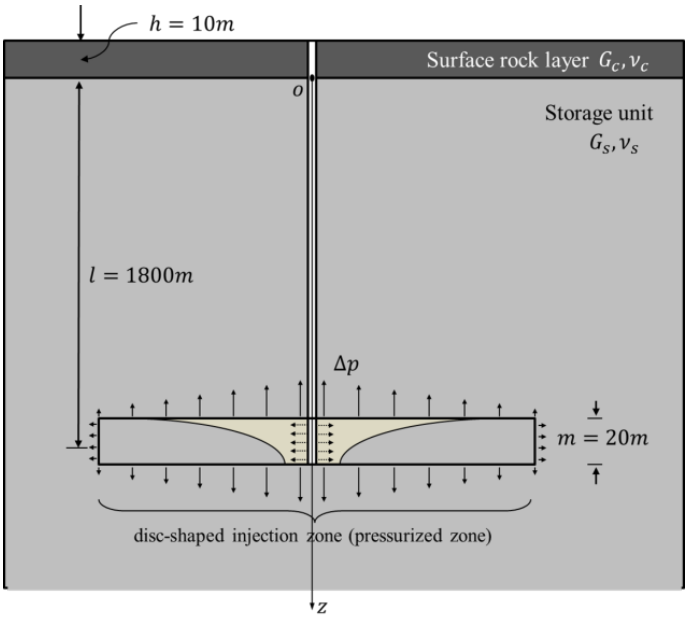

Figure 9 Geometry of the model to simulate the surface uplift around the injection well KB501 at In Salah

To evaluate the surface uplift, the geometry shown in **Figure 9** is used. The system includes a 10 m thick thin surface layer and an injection zone that is within a storage unit. The injection zone is located 1800m below the surface rock layer. The overburden unit is actually eliminated. The problem is therefore to assess the interaction between a bonded surface rock layer and a deep storage unit, while CO_2 is injected at a certain depth within the storage unit.

Material properties of the injection zone are directly taken from [6] (**Table 2**) and the mechanical properties of the storage unit also correspond to the mean value of material sets in [6].

Table 2 Material parameters used in the simulation of In Salah uplift

Parameter	Unit	Storage unit	Surface layer
Shear modulus	GPa	3	0.5
Poisson's ratio	-	0.2	0.2
Porosity in the injection zone	-	0.17	-
Permeability in the injection zone	m^2	1.3e-14	-

Figure 10 shows good agreement of the results between the semi-analytical solution and the actual measurements. The model reproduces about an 11mm surface uplift in the first year while the detected surface uplift was around 10mm (**Figure 8**b). After 3 years of injection, the maximum calculated uplift is 16mm, which is similar to the measured uplift (15mm) (**Figure 8**b). Using the 3D finite element model, Rutqvist *et al.* [6] also found a surface uplift of 12mm, which is in the same order of magnitude as that found with the semi-analytical solution. In terms of the fluid pressure, the overpressure around the injection well, 14MPa with the NB and 15MPa with the DZ solution, is predicted by the semi-analytical solution; this is also similar to the overpressure calculated by the finite element simulation of from [6].

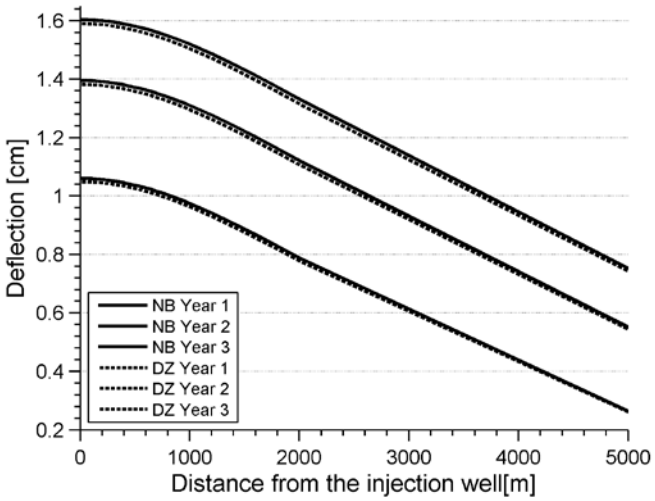

Figure 10 Surface uplift calculated by the semi-analytical solution

5. CONCLUSION

This paper presents a semi-analytical approach to estimate the caprock deflection due to CO_2 injection. The model examines the interaction between a primary caprock and adjacent regions with elastic material properties, which is induced by the pressurization within the injection zone. Using the embedded plate approach, the primary caprock is modelled as a thin-plate layer and adjacent regions are modelled as semi-infinite half-space regions. For the fluid part, two analytical solutions have been introduced into this approach. The expressions have been derived in order to develop a compact analytical solution. This approach can take into account a moving front of immiscible fluids and a more realistic fluid pressure distribution. Several numerical experiments have been undertaken to illustrate the influence of factors such as geometry, overpressure magnitude and material properties on the caprock deflection. Finally we employ this approach to assess the surface uplift observed at In Salah. A good agreement in the temporal evolution and the magnitude has been found between the measurements and calculated results. Compared to finite element calculations, this approach can be considered as an alternative preliminary calculation tool for assessing the impact of various factors during CO_2 injection.

The development within this paper is straightforward. One can incorporate other analytical solutions in relation to the fluid dynamics into the mechanical approach. Thus, advances in hydrology research can also be of benefit to this approach.

ACKNOWLEDGMENT

The authors gratefully acknowledge Petrosvibri S.A. for funding of the Chair “Gaz Naturel” and supporting this research.

REFERENCES

1. D. Reichle, J. Houghton, B. Kane, and J. Ekmann, "Carbon sequestration research and development" Oak Ridge National Lab., TN (US); National Energy Technology Lab., Pittsburgh, PA (US); National Energy Technology Lab., Morgantown, WV (US)1999.
2. E. Bryant and E. A. Bryant, *Climate Process & Change*: Cambridge Univ Pr, 1997.
3. S. Bachu, "Sequestration of CO_2 in geological media: criteria and approach for site selection in response to climate change," *Energy Conversion and Management*, vol. 41, pp. 953-970, 2000.
4. T. Onuma and S. Ohkawa, "Detection of surface deformation related with CO_2 injection by DInSAR at In Salah, Algeria," *Energy Procedia*, vol. 1, pp. 2177-2184, 2009.
5. D. Vasco, A. Ferretti, and F. Novali, "Reservoir monitoring and characterization using satellite geodetic data: Interferometric synthetic aperture radar observations from the Krechba field, Algeria," *Geophysics*, vol. 73, pp. WA113-WA122, 2008.
6. J. Rutqvist, D. W. Vasco, and L. Myer, "Coupled reservoir-geomechanical analysis of CO_2 injection and ground deformations at In Salah, Algeria," *International Journal of Greenhouse Gas Control*, vol. 4, pp. 225-230, 2010.
7. V. Vilarrasa, D. Bolster, S. Olivella, and J. Carrera, "Coupled hydromechanical modeling of CO_2 sequestration in deep saline aquifers," *International Journal of Greenhouse Gas Control*, vol. 4, pp. 910-919, 2010.
8. J. Rutqvist, "The geomechanics of CO_2 storage in deep sedimentary formations," *Geotechnical and Geological Engineering*, vol. 30, pp. 525-551, 2012.
9. J. Rohmer and D. M. Seyedi, "Coupled large scale hydromechanical modelling for caprock failure risk assessment of CO_2 storage in deep saline aquifers," *Analyse hydromècanique á grande èchelle pour l'èvaluation du risque de fracturation de la couverture de stockage du CO_2 dans les aquifères profonds*, vol. 65, pp. 503-517, 2010.
10. P. S. Ringrose, A. S. Mathieson, I. W. Wright, F. Selama, O. Hansen, R. Bissell, N. Saoula, and J. Midgley, "The In Salah CO_2 storage project:

lessons learned and knowledge transfer," *Energy Procedia*, 2013.
11. E. Fjaer, *Petroleum Related Rock Mechanics*: Elsevier Science, 2008.
12. A. P. S. Selvadurai, "Heave of a surficial rock layer due to pressures generated by injected fluids," *Geophysical Research Letters*, vol. 36, L14302, doi:10.1029/2009GL038187, 2009.
13. A. P. S. Selvadurai, "Mechanics of an embedded caprock layer during pressurization of a CO_2 reservoir, *Proceedings of ComGeo 09: Computational Geomechanics I* (S. Pietruszczak, G.N. Pande, C. Tamagnini and R. Wan, Eds.) Int. Centre for Comp. Eng., pp. 466-475." 2009.
14. V. Vilarrasa, D. Bolster, M. Dentz, S. Olivella, and J. Carrera, "Effects of CO_2 compressibility on CO_2 storage in deep saline aquifers," *Transport in Porous Media*, vol. 85, pp. 619-639, 2010.
15. J. M. Nordbotten, M. A. Celia, and S. Bachu, "Injection and storage of CO_2 in deep saline aquifers: Analytical solution for CO_2 plume evolution during injection," *Transport in Porous Media*, vol. 58, pp. 339-360, 2005.
16. M. Dentz and D. M. Tartakovsky, "Abrupt-interface solution for carbon dioxide injection into porous media," *Transport in Porous Media*, vol. 79, pp. 15-27, 2009.
17. A. Selvadurai, *Partial Differential Equations in Mechanics 2: The Biharmonic Equation, Poisson's Equation* vol. 2: Springer, 2000.
18. P. Segall, J.-R. Grasso, and A. Mossop, "Poroelastic stressing and induced seismicity near the Lacq gas field, southwestern France," *Journal of Geophysical Research: Solid Earth*, vol. 99, pp. 15423-15438, 1994.
19. J. Geertsma, "Land subsidence above compacting oil and gas reservoirs," *Journal of Petroleum Technology*, vol. 25, pp. 734-744, 1973.
20. J. Bear, "*Dynamics of Flow in Porous Media*," ed: Elsevier, New York, 1972.
21. C. Lu, S. Y. Lee, W. S. Han, B. J. McPherson, and P. C. Lichtner, "Comments on “abrupt-interface solution for carbon dioxide injection into porous media” by M. Dentz and D. Tartakovsky," *Transport in Porous Media*, vol. 79, pp. 29-37, 2009.
22. M. Dentz and D. M. Tartakovsky, "Response to “Comments on abrupt-interface solution for carbon dioxide injection into porous media by Dentz and Tartakovsky (2008)” by Lu et al," *Transport in Porous Media*, vol. 79, pp. 39-41, 2009.
23. V. Oye, P. Zhao, D. Khn, K. Iranpour, E. Aker, and B. Bohloli, "Monitoring of the In Salah CO_2 storage site (Krechba) using microseismic data analysis," *3rd EAGE CO_2 Geological Storage Workshop, Edinburgh.*, 2012.
24. B. Bohloli, E. Aker, F. Cuisiat, V. Oye, and D. Khn, "Analysis of pressure versus flow regime of CO_2 to assess matrix and fracture injection at In Salah, Algeria," *3rd EAGE CO_2 Geological Storage Workshop, Edinburgh.*, 2012.
25. J. Rutqvist, D. W. Vasco, and L. Myer, "Coupled reservoir-geomechanical analysis of CO_2 injection at In Salah, Algeria," *Energy Procedia*, vol. 1, pp. 1847-1854, 2009.

APPENDIX I

The Bessel functions are the canonical function solutions of the following equation:

$$x^2\frac{d^2y}{dx^2}+x\frac{dy}{dx}+(x^2-\alpha^2)y=0$$

where α is a real or complex number and refers to the order of the Bessel function.

The function J_α denotes the Bessel function solution of the previous equation. Functions of concern here are those that are finite at the origin (for an integer or positive α) and these diverge as x approaches zero (for negative non-integer α), so that this solution is called the Bessel function of first kind of order α.

Let’s assume α be an integer. We have the following recurrence properties for α=n (n is an integer):

$$J_{n+1}(x)=\frac{nJ_n(x)}{x}-J'_n(x)$$

$$J_{n+1}(x)+J_{n-1}(x)=\frac{2nJ_n(x)}{x}$$

$$J_{n+1}(x)-J_{n-1}(x)=-2J'_n(x)$$

Hence, one has

$$J_1(x)=-J'_0(x)$$

$$\frac{d}{dx}(x^nJ_n(x))=x^nJ_{n-1}(x)$$

APPENDIX II

We have seen in the first part of this work that it is common to approximate $\int_{l-m/2}^{l+m/2} e^{-kd}\,\mathrm{d}d \approx me^{-kl}$ by te^{-kd}.

This stems from the fact that the hyperbolic sinus $sh(x)\approx x$ when x is sufficiently small. But in our case,

it leads to the approximation: $sh(kt/2) \approx kt/2$. However k varies from 0 to infinity and t is a constant. The approximation we did previously needs to be verified.

It is necessary to look at all the integrals composing the $u_z^{(s)p}$ term.

We have:

$$u_z^{(s)p}(r,0) = \frac{b}{G_s}\int_0^\infty\int_0^\infty p(\rho)\cdot g_z(r,z=0;\rho,d)\,\mathrm{d}\rho\,\mathrm{d}d$$

with:

$$g_z(r,z=0;\rho,d) = -(1-2\nu_s)\rho\int_0^\infty \xi J_0(\xi r)J_0(\xi\rho)e^{-\xi d}\,\mathrm{d}\xi$$

For simplification and without any loss of generality, we assume that the pressure is constant over a radius R from the injection well (otherwise we work with an inequality and the maximum pressure over the domain).

$$P(r,z) = \Delta P\, H(R-\rho)\ if\ d-\frac{t}{2} \le z \le d+\frac{t}{2}$$

$$P(r,z) = 0 \quad otherwise$$

This gives:

$$u_z^{(s)p}(r,0) = -\frac{(1-2\nu_s)b\Delta PR}{G_s}$$

$$\times\int_0^\infty J_0(kr)J_1(kR)\frac{2}{k}e^{-kl}sh\left(\frac{kt}{2}\right)dk \equiv u$$

If we had done the previous approximation, we would have found the same result as the Eq.(10) in [18]:

$$u_z^{(s)p}(r,0) = -\frac{(1-2\nu_s)b\Delta PR}{G_s}$$

$$\times\int_0^\infty t\,J_0(kr)J_1(kR)e^{-kl}dk \equiv \tilde{u}$$

Setting $C = -\frac{(1-2\nu_s)b\Delta PR}{G_s}$, we have:

$$(u-\tilde{u})(r) = C\int_0^\infty\left(\frac{2}{k}sh\left(\frac{kt}{2}\right)-t\right)J_0(kr)J_1(kR)e^{-kl}dk$$

To study the problem, we look at the behaviour of the previous function, depending on r, throughout the numerical computation. For the best computation, we can change the variable:

$$\mathbb{R}^+ \to [0;1[$$

$$\varphi : y \to argth(y) = \frac{1}{2}\ln\left(\frac{1-y}{1+y}\right)$$

This gives:

$$(u-\tilde{u})(r) = -C\int_0^1\left(\begin{array}{l}\left(\frac{2}{argth(y)}sh\left(\frac{argth(y)t}{2}\right)-t\right)\\ \times J_0(argth(y)r)\,J_1(argth(y)R)\\ \times e^{-argth(y)l}\,\frac{y}{1-y^2}\end{array}\right)dy$$

We observe that the difference is very small (around 10^{-13}) compared to the value of u or $\tilde{u}$ (around $10^{-2} \sim 10^{-3}$) as shown in the figure below.

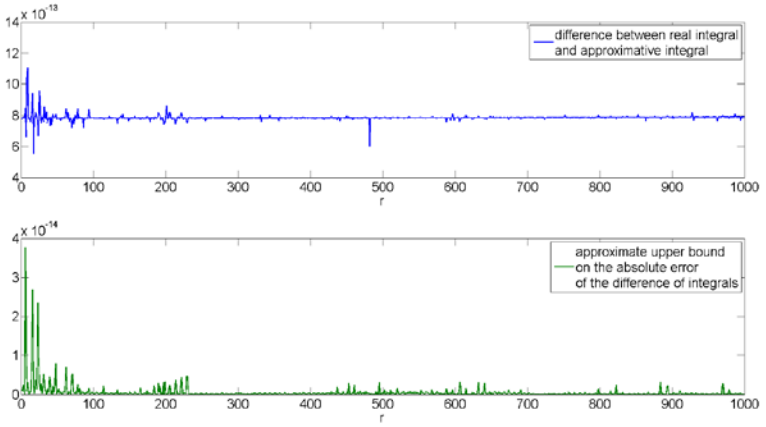

APPENDIX III

The Hankel transform expresses any given function f as the weighted sum of an infinite number of Bessel functions of the first kind.

That is to say, the Hankel transform of order α of a function f is defined as (with $\alpha \ge \frac{1}{2}$):

$$F_\alpha(k) = \int_0^\infty rf(r)J_\alpha(kr)dr, k \in \mathbb{R}^+$$

And the inverse Hankel transform is given by:

$$f(r) = \int_0^\infty kF_\alpha(k)J_\alpha(kr)dk, r \in \mathbb{R}^+$$

It is worthwhile to note that the Hankel transform of order zero is essentially the two dimensional Fourier transform in cylindrical coordinates.